Highly Efficient Visible Light Photocatalytic Reduction of CO2 to Hydrocarbon Fuels by Cu-NPs Decorated Graphene Oxide

ARTICLE *in* NANO LETTERS · OCTOBER 2014

Impact Factor: 13.59 · DOI: 10.1021/nl503609v

CITATIONS
12

READS
63

14 AUTHORS, INCLUDING:

Indrajit Shown
Academia Sinica
17 PUBLICATIONS **162** CITATIONS
SEE PROFILE

Pradip kumar Roy
Academia Sinica
8 PUBLICATIONS **23** CITATIONS
SEE PROFILE

Abhijit Ganguly
Academia Sinica
40 PUBLICATIONS **1,175** CITATIONS
SEE PROFILE

NANO LETTERS

Letter

pubs.acs.org/NanoLett

Highly Efficient Visible Light Photocatalytic Reduction of CO_2 to Hydrocarbon Fuels by Cu-Nanoparticle Decorated Graphene Oxide

Indrajit Shown,[†] Hsin-Cheng Hsu,[†,‡] Yu-Chung Chang,[‡] Chang-Hui Lin,[‡] Pradip Kumar Roy,[§,⊥] Abhijit Ganguly,[†] Chen-Hao Wang,[‡] Jan-Kai Chang,[∥] Chih-I Wu,[∥] Li-Chyong Chen,*[,§] and Kuei-Hsien Chen*[,†,§]

[†]Institute of Atomic and Molecular Sciences, Academia Sinica, Taipei 10617, Taiwan

[‡]Department of Materials Science and Engineering, National Taiwan University of Science and Technology, Taipei 10607, Taiwan

[§]Center for Condensed Matter Sciences, National Taiwan University, Taipei 10617, Taiwan

[⊥]Institute of Biophotonics, National Yang Ming University, Taipei 112, Taiwan

[∥]Department of Electrical Engineering, National Taiwan University, Taipei 10617, Taiwan

Supporting Information

ABSTRACT: The production of renewable solar fuel through CO_2 photoreduction, namely artificial photosynthesis, has gained tremendous attention in recent times due to the limited availability of fossil-fuel resources and global climate change caused by rising anthropogenic CO_2 in the atmosphere. In this study, graphene oxide (GO) decorated with copper nanoparticles (Cu-NPs), hereafter referred to as Cu/GO, has been used to enhance photocatalytic CO_2 reduction under visible-light. A rapid one-pot microwave process was used to prepare the Cu/GO hybrids with various Cu contents. The attributes of metallic copper nanoparticles (~4−5 nm in size) in the GO hybrid are shown to significantly enhance the photocatalytic activity of GO, primarily through the suppression of electron−hole pair recombination, further reduction of GO's bandgap, and modification of its work function. X-ray photoemission spectroscopy studies indicate a charge transfer from GO to Cu. A strong interaction is observed between the metal content of the Cu/GO hybrids and the rates of formation and selectivity of the products. A factor of greater than 60 times enhancement in CO_2 to fuel catalytic efficiency has been demonstrated using Cu/GO-2 (10 wt % Cu) compared with that using pristine GO.

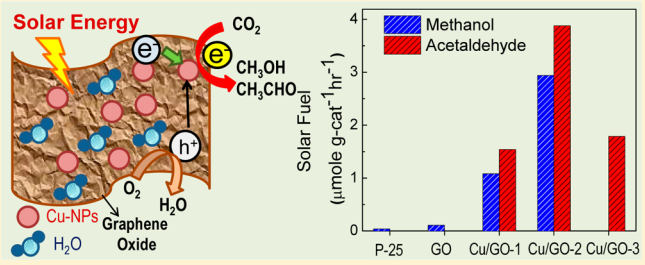

KEYWORDS: *graphene oxide, copper nanoparticle, photocatalyst, CO_2 photoreduction, solar fuel, artificial photosynthesis*

The rising demand for fossil fuels in our modern society results in emissions of vast quantities of carbon dioxide (CO_2) in the atmosphere. This increasing CO_2 concentration in air is the most serious environmental concern associated with global warming and climate change.[1] Therefore, finding a way for conversion of CO_2 into fuel (energy) is highly desirable for sustainable energy production. Toward this goal, biomimetic artificial photosynthesis has recently gained attention as a promising technology for reduction of CO_2 to fuel using solar energy. In this process, the hydrocarbons are produced by photoreduction of CO_2 using water and solar energy.[2,3] In 1979, Inoue et al. first demonstrated the photocatalytic reduction of carbon dioxide to form organic compounds by using a photosensitive semiconductor.[4] After this pioneering breakthrough, several wide-bandgap semiconductor materials have been explored toward the photocatalytic CO_2 reduction.[5−11] Among all these semiconductor materials, titanium dioxide (TiO_2) and some TiO_2-based heterogeneous photocatalysts have been explored most extensively due to their low cost and high chemical stability.[12,13] Several other nontitanium metal oxide,[14] metal sulfides,[15] and few homogeneous organometallic materials[16−19] also have been demonstrated as potential photocatalyst materials for CO_2 reduction. Several studies have shown that the catalytic efficiency for CO_2 reduction is compromised due to the high electron−hole recombination rates in the semiconductor materials and low visible-light absorption in wide-bandgap semiconductors. To overcome these, several strategies have been employed to enhance the photocatalytic activity of wide-bandgap semiconductor materials.[20−22] One of the most popular techniques is to modify the semiconductor with noble metal cocatalyst that acts as an electron acceptor, and in-turn suppresses the recombination of photo excited electron−hole pairs.[23,24] However, the challenge remains due to the low quantum efficiency of electron acceptance by the cocatalyst and lack of selectivity in the production of fuels. Thus, it is highly desirable

Received: May 26, 2014
Revised: October 20, 2014
Published: October 29, 2014

to develop a potential photocatalyst at low cost to achieve high CO_2 reduction efficiency to produce fuel using just the sunlight.

The graphene oxide (GO) is a highly attractive low cost two-dimensional nanostructured oxide of graphite. It is basically an atomically thin carbon sheet with various oxygenated functional groups on the basal plane and peripheries.[25,26] The various isolated oxygenated functional groups and stoichiometric C/O ratio on the basal plane make GO partially insulating wide-bandgap semiconductor like material.[27,28] These semiconductor-like characteristics of the wide-bandgap material GO make it a promising potential candidate for photocatalyst.[29,30] Recently, it has been reported that reduced GO-based composite material can be a promising photocatalyst, where the GO acts as a hole collecting material and reduces the electron−hole recombination.[31−33]

In 2010, Yeh et al. demonstrated GO as an active photocatalyst for water splitting application.[34] In our previous study, we demonstrated that tunable band gap GO is a promising photocatalyst for CO_2 to methanol conversion under solar irradiation.[35] Despite yielding a 6-fold enhancement over commercial P-25 catalyst, the CO_2 to methanol conversion efficiency using GO is still insufficient for practical applications due to the six-electron process involved in the catalysis and high rates of recombination of the photogenerated electron−hole pairs. For GO, though the superior to TiO_2 performance is encouraging, its bandgap is still too large for the visible-light response. Therefore, further studies are needed to better the understanding of the mechanism of GO-based photocatalysis reaction to lead to development of a viable technology.

In this present work, metal nanoparticle (NP) with control size distribution is incorporated in GO, forming a heterogeneous catalyst to enhance CO_2 photoreduction efficiency. Cu, in particular, has been chosen as the cocatalyst due to its known effectiveness in CO_2 and hydrocarbon catalytic reaction, the large work function of Cu compared to that of GO,[36−38] and a possible formation of Schottky junction between Cu and GO to enhance the separation of photo generated electrons and holes. The catalytic effect of copper in electrochemical reduction of CO_2 has been extensively investigated by Hori et al., which resulted in a large range of hydrocarbon products.[39,40] Gattrell et al.[41] have also demonstrated electrocatalytic reduction of CO_2 to hydrocarbons on the selective copper crystal surface. Therefore, we considered that variations in Cu fraction in the GO-based hybrids photocatalyst would be capable of tuning the redox potentials of GO to achieve enhanced CO_2 photocatalysis and may result in highly selective generation of hydrocarbons as solar fuels from CO_2.

In the present study, a series of GO decorated with Cu-NPs (hereafter referred to as Cu/GO) composites with different fractions of Cu nanocrystals were synthesized using a single pot microwave method. The effects of variations in Cu content on the crystal structure, morphology, optical properties, and photocatalytic activity of the Cu/GO hybrids were systematically investigated. In particular, we show that there exists an optimum Cu content and its size distribution within the Cu/GO composite that results in maximum solar fuel generation efficiency. Detailed investigations on the optimum cocatalyst (Cu) content, its size distribution, and a possible mechanism for the selective solar fuel generation are presented here.

A typical one-pot microwave process for synthesis of Cu/GO hybrid is presented schematically in Figure 1a. GO was mixed ultrasonically with metal precursor $Cu(NO_3)_2{\cdot}3H_2O$ in ethylene glycol, followed by microwave heating to yield the Cu/GO

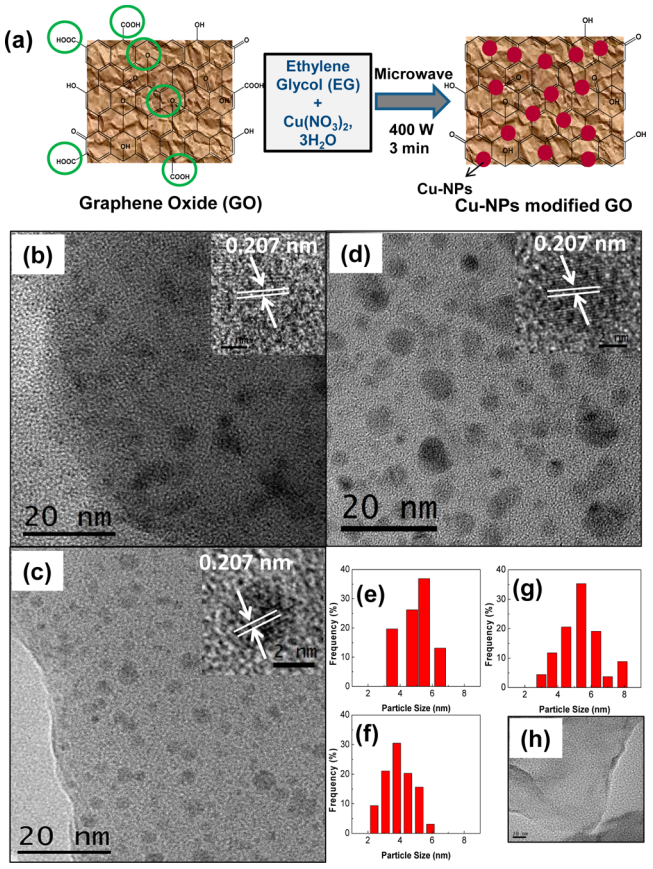

Figure 1. (a) Scheme presentation of the microwave synthesis process for GO hybrids decorated with Cu-NPs. (b−d) TEM images of Cu/GO-1, Cu/GO-2, and Cu/GO-3. Inset: HRTEM image of single Cu-NP of the respective Cu/GO hybrids, respectively. (e−g) Size distribution of Cu-NPs in Cu/GO-1, Cu/GO-2, and Cu/GO-3, respectively. (h) Representative TEM image of GO.

composite, resulting from simultaneous reduction of Cu precursor to form Cu nanoparticles on the GO surface. The originally yellow colored GO was transformed into black-colored partially modified GO after the microwave treatment, which was confirmed by the XPS analysis. The desired Cu content in the Cu/GO hybrids was controlled from 5 to 15 wt % as determined by EDX analysis (see Supporting Information Figure S1). These Cu-NPs-modified GOs are denoted as Cu/GO-1 (5 wt % Cu), Cu/GO-2 (10 wt % Cu), and Cu/GO-3 (15 wt % Cu), with measured Cu loading of 4.12, 9.52, and 15.16 wt %, respectively (Table 1).

The phase structures of unmodified GO and Cu/GOs hybrids were examined by X-ray diffraction (XRD) measurement. Supporting Information Figure S2a−d compares the XRD patterns of pristine GO and Cu/GO hybrids in the range of 5°−70° (2θ). In Supporting Information Figure S2a, the characteristic broad (002) peak corresponding to GO was observed at a diffraction angle of 11.3°, which represents complete oxidation of graphene oxide. The observed increase in d spacing of GO sheets is believed to be due to the presence of abundant oxygen moieties on both sides of the graphene sheet, causing an atomic-scale roughness on the graphene surface. As shown in Supporting Information Figure S2b−d, the Cu/GO hybrids exhibit an additional peak at around 42.88° that corresponds to metallic copper (111), and no signs of formation of any copper oxides, indicating that Cu ions were

dx.doi.org/10.1021/nl503609v | Nano Lett. 2014, 14, 6097−6103

Table 1. Effects of Cu Content and Particle Size on Photophysical Properties of the Cu/GO Samples

samples	Cu content (wt %) nominal	Cu content (wt %) calculated by EDX	grain size[a] (nm)	average particle size[b] (nm)	band gap[c] (eV)	D band (cm^{-1})	G band (cm^{-1})	I_D/I_G
GO	0				3.28−3.93	1347.01 ± 0.31	1577.43 ± 0.33	1.44
Cu/GO-1	5	4.12 ± 0.70	4.21	5.06 ± 1.3	2.69−3.13	1338.51 ± 0.23	1592.54 ± 0.21	1.43
Cu/GO-2	10	9.52 ± 0.75	4.07	4.15 ± 1.3	2.51−3.09	1339.24 ± 0.20	1595.27 ± 0.26	1.44
Cu/GO-3	15	15.16 ± 0.62	4.64	5.39 ± 1.7	2.41−3.07	1337.25 ± 0.22	1596.32 ± 0.20	1.39

[a]Average crystallite size is determined by the Cu (111) face diffraction peak using Scherrer formula. [b]Average particle size calculated from the TEM. [c]Calculation based on Tauc plot.

thermally reduced during the microwave process. The GO (002) peak in the modified materials is seen to shift to slightly higher diffraction angle at 12.6°, which is mainly attributed to partial modification of pristine GO during microwave treatment. Additionally, the average crystalline size of Cu NPs in the various Cu/GO hybrid samples was calculated using the Scherrer formula for Cu (111) phase diffraction peak as listed in Table , yielding the crystal sizes of 4.21, 4.07, and 4.67 nm for Cu/GO-1, Cu/GO-2, and Cu/GO-3, respectively.

The morphology and microstructure of the samples were investigated using transmission electron microscopy (TEM) as shown in Figure 1b−d, revealing that the Cu nanoparticles are distributed uniformly on GO, which is facilitated by the widespread presence of oxygen containing functional groups on GO. It was also observed in all the images that the Cu nanoparticles have formed some small clusters on GO. The TEM images and particle size distribution histograms (Figure 1e−g) of the Cu/GO show an average size of 5.06 ± 1.3, 4.15 ± 1.3, and 5.36 ± 1.7 nm for Cu/GO-1, Cu/GO-2, and Cu/GO-3, respectively, which is highly consistent with the cluster size values obtained via the Scherrer formula (Table 1) from XRD analysis. In contrast, Figure 1h shows a 2D layer-by-layer structure of stacked nano sheet of pristine GO. It is observed that, with an increase in Cu content, the particle size distribution becomes broader and lattice fringes corresponding to Cu(111) fcc structure can be clearly identified.

UV−vis spectroscopy study was also carried out in order to understand the optical properties of the GO based photocatalyst. Supporting Information Figure S3 shows the normalized absorption spectra of GO and Cu/GO hybrids. In Supporting Information Figure S3a, graphene oxide shows the characteristic absorption near 200 nm with a small shoulder at 300 nm. The absorption band at 200 nm is mainly attributed to the $\pi \rightarrow \pi^*$ transition of C═C in graphitic structure, whereas the small shoulder at 300 nm is due to the $n \rightarrow \pi^*$ transition of C═O. The UV−vis spectra of Cu/GOs (5 wt % Cu, 10 wt % Cu, and 15 wt % Cu), presented in Supporting Information Figure S3b−d, display typical absorption bands around 200 to 280 nm and the characteristic absorption from small Cu nanoparticles (Cu-NPs) clusters[42] at around 286 nm. However, no localized surface plasmon Cu peak is observed at around 550 nm. This typical characteristic in the UV−vis spectra of Cu/GO hybrids confirms the formation of Cu-NPs of less than 10 nm in size.[43] This result is consistent with the results from XRD and TEM analyses. From the Tauc plot in the inset of Supporting Information Figure S3, approximate bandgaps of 3.28−3.89, 2.69−3.13, 2.51−3.09, and 2.41−3.07 eV for GO, Cu/GO-1, Cu/GO-2, and Cu/GO-3, respectively, were obtained. It is observed that copper modification greatly enhanced the optical absorption in graphene oxide in the visible-light region. However, the decrease in bandgap of GO with increasing Cu concentration is not well understood. We attribute the bandgap shift to the interaction of copper ions with the oxygenated functional groups on GO.

The structural modification of the GO and Cu/GOs composites have been studied by Raman spectroscopy. As shown in Supporting Information Figure S4, the G band in all of the Cu/GO hybrids is blue-shifted in comparison to that of the pristine graphene oxide at ∼1596 cm^{-1}, indicating the relaxation of compressive strain in the pristine GO sheet due to modification with Cu NPs. The red shift of the D band in Cu/GO hybrids compared to pristine GO could be attributed to the doping effect of metallic Cu on graphene oxide. Further increasing of Cu content on GO led to change in the I_D/I_G ratio as listed in Table 1. The typical I_D/I_G ratio confirms the defect density in GO and Cu/GO, which originates from defects associated with vacancies, grain boundaries, and amorphous carbons.

Elemental compositions of the pristine GO and Cu/GO hybrids were determined using X-ray photoemission spectroscopy (XPS) analysis. Figure 2 shows the C 1s and Cu 2p XPS spectra of the samples. The C 1s band of GO (Figure 2a) exhibits the five components at 284.6, 285.6, 286.9, 288.3, and 288.9 eV corresponding to C—C/C═C in aromatic rings, C—OH (hydroxyl), C—O—C (epoxy, ether), >C═O (carbonyl, ketone), and —COOH (carboxylic) groups, respectively. In Figure 2b−d the C 1s XPS spectra of Cu/GO composites is shown, deconvoluted into four peaks at 284.2, 285.6, 286.9, and 288.3 of C═C/C—C, C—OH, C—O—C, and >C═O, respectively. The C 1s XPS spectra of Cu/GO composites showed a significant decrease in the relative intensity of the oxygen containing functional groups (—COOH and C—O—C) as a result of the partial modification of GO. Interestingly, it can be noted that a small downshift of C═C peak is observed in Cu/GO composites as compared to pristine GO. This could be reasonably attributed to the interfacial charge transfer from GO to Cu nanocrystal. A similar charge transfer phenomenon has been previously reported by Koroteev et al.[44] in their metal-sulfide/CNT composite. We expect such an interfacial charge transfer to help improve the photocatalytic performance of Cu/GO hybrids. It may noted that, the intensity of the C—C/C═C peak increased in the composites, along with a dramatic decrease in the overlapping peaks at 285.6−288.9 eV. In Figure 2e−g Cu 2p spectra of all Cu/GO hybrids show strong peak at 932.6 eV, which perfectly matched with the binding energy of Cu $2p_{3/2}$ of Cu° state. The small shoulder at 935 eV on the higher binding energy side of Cu $2p_{3/2}$ indicates the presence of a very small amount of divalent state of copper on the surface of the metallic Cu-NPs clusters. The XPS spectra of Cu/GO hybrids with various fractions of Cu loading in Figure 2e−g

dx.doi.org/10.1021/nl503609v | Nano Lett. 2014, 14, 6097−6103

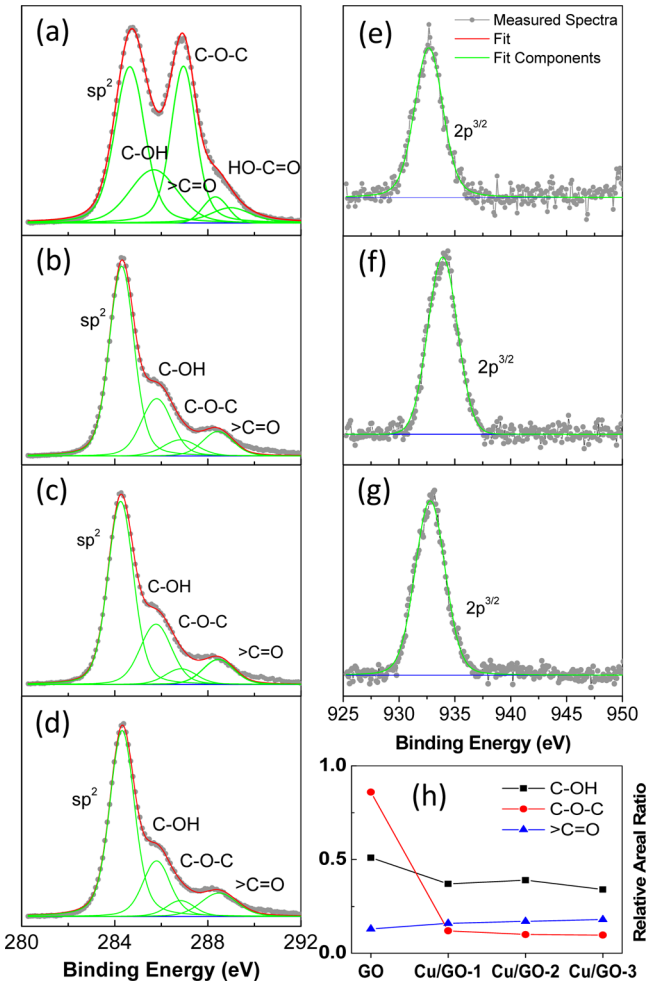

Figure 2. High-resolution XPS spectra of: (a–d) C 1s for GO, Cu/GO-1, Cu/GO-2, and Cu/GO-3; (e–g) corresponding Cu $2p_{3/2}$ for Cu/GOs. (h) Relative areal intensity of —C—OH, >C═O and —C—O—C, normalized with the sp^2 components.

indicate that Cu° is the dominant state in these hybrids. The correlation between the relative peak intensities of the three C 1s components, as illustrated in Figure 2h, provides better understanding of the partial modification of GO during the microwave process. It is observed that in Cu/GO hybrids, the relative intensity of C—O—C oxygenated functional groups decrease significantly compared to that in the pristine GO, whereas the intensity of >C═O and —C—OH functional groups change very little. The XPS analysis thus leads to a conclusion that the oxygen containing —COOH and C—O—C functional groups have been removed completely or partially form GO during the microwave synthesis process. Similarly, from the O 1s XPS spectra of GO and Cu/GO composites presented in Supporting Information Figure S5 show complete removal of —COOH functional groups and partial removal of the C—O—C and C—OH functional groups in Cu/GOs composites after partial modification of GO. It should be noted that the oxygen XPS peaks are dominated by the C—O—C and other related functional groups, but no detectable additional peak due to oxidation of Cu surface is present. This can be explained by considering that the total amount of incorporated Cu, and therefore CuOx, is relatively small compared to GO.

Finally, the photocatalytic activity of the Cu/GO hybrids and pristine GO toward gas-phase CO_2 photoreduction under visible light irradiation was experimentally determined. Methanol and acetaldehyde are found to be the major products and hydrogen as a minor product of CO_2 photoreduction. However, due to the detection limit of the GC column, we were unable to detect very low concentration of hydrogen as compared to the other major products CH_3OH and CH_3CHO. The rates of formation of CH_3OH and CH_3CHO on the synthesized photocatalyst as afunction of irradiation times are plotted in Figure 3. It is observed that the acetaldehyde

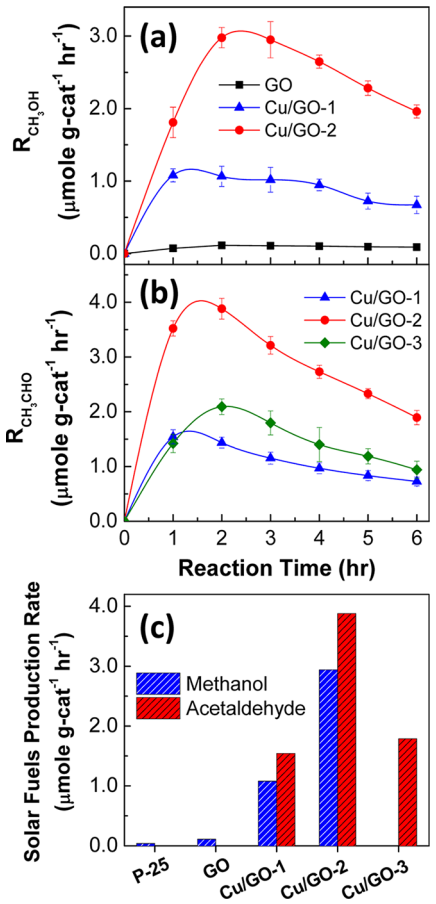

Figure 3. Production rates of (a) methanol (b) acetaldehyde on the pristine GO, Cu/GO-1, Cu/GO-2, and Cu/GO-3 as a function of irradiation time. (c) Solar fuel production rate for GO, and Cu/GO-1, Cu/GO-2, and Cu/GO-3 (production rate was derived following 2 h of light irradiation).

formation on Cu/GO hybrid is more favorable compared to methanol formation. Interestingly, Figure 3 shows that the production rates of solar fuel increase with the increase in Cu loading on GO photocatalyst from 5 wt % to 10 wt %. However, Figure 3 also shows that the catalytic performance decreases in the presence of Cu over loading (15 wt %) on GO (Cu/GO-3). The highest methanol and acetaldehyde production rate are achieved with 10 wt % of Cu in GO (Cu/GO-2). The Cu/GO-3 composite with 15 wt % of Cu shows only acetaldehyde formation. The methanol production rates for the photocatalyst Cu/GO-1, Cu/GO-2, and Cu/GO-3 are 1.08, 2.94, and 0 μmol g-cat^{-1} h^{-1} after 2 h irradiation, whereas the calculated acetaldehyde production rates are 1.54, 3.88, and 1.79 μmol g-cat^{-1} h^{-1} for Cu/GO-1, Cu/GO-2, and Cu/GO-3,

dx.doi.org/10.1021/nl503609v | Nano Lett. 2014, 14, 6097–6103

respectively. Further, Figure 3 also shows a slight decline in product formation rate for all Cu/GO hybrids after a few hours, which is presumably due to the deterioration of photocatalyst and reoxidation of methanol. Figure 3c presents the total solar fuel (methanol and acetaldehyde) formation rate for a 2 h irradiation on Cu/GO hybrids with different Cu contents, along with the corresponding rates for pristine GO and commercial TiO_2 (P-25). The pristine GO shows a very low photocatalytic solar fuel production rate of 0.11 μmol g-cat^{-1} h^{-1}. The loading of Cu-NPs cocatalyst results in a significant improvement in the photocatalytic solar fuel production rate of GO. In the presence of 5 wt % of Cu-NPs in GO (Cu/GO-1), the solar fuel production rate is increased to 2.64 μmol g-cat^{-1} h^{-1}. With an increase in Cu-NPs loading to 10 wt % (Cu/GO-2), the solar fuel production rate achieves the highest value of 6.84 μmol g-cat^{-1} h^{-1}, which is more than 60 times that of pristine GO, or 240 times that of P-25. Notably, to the best of our knowledge, this is the highest rate of photocatalytic CO_2 reduction ever reported in the literature.

It is well known that the photocatalytic CO_2 reduction mainly involves generation of charge carriers, charge carrier transfer, and finally, multielectron chemical reduction on a particular potential. In an initial step of charge carrier generation, GO decorated with Cu-NPs is excited by visible light, photons with higher energy than the band gap of the GO generate electron−hole pairs on the Cu/GO photocatalyst surface. Next, on the GO photocatalyst surface, Cu-NPs act as the electron acceptor and suppress the recombination of photo excited electron−hole pair due to enhanced charge separation at the metal−semiconductor interface. Finally, the activation of CO_2 is more effectively performed on the Cu-NPs decorated GO surface due to the transfer of an electron from the metal d orbital to the (C−O) π^* orbital.[45] Consequently, the favorable multielectron reduction process involves breaking of C−O bonds and formation of C−H bonds, leads to creation of methanol and acetaldehyde as major product and hydrogen as minor product. Although the hydrogen evolution reaction may compete with the CO_2 reduction reaction, the fact that hydrogen was barely detectable as a product indicates that it is indeed a minor reaction. In fact, surface activation energy of the Cu in the volcano plot[46] indicates unfavorable conditions for the photogenerated electrons to interact with the protons to form H_2. Recently, Shi et al.[47] have demonstrated theoretically that adsorption of CO and intermediates on Cu (111) surface can be favorable for hydrocarbon formation from the CO_2 reduction reaction, which clearly supports our experimental observation of favorable CO_2 reduction to hydrocarbons on the Cu-NPs (111) decorated GO surface. Specifically, six-electron and ten-electron reduction processes are involved in the production of methanol and acetaldehyde, respectively, in our experiment. The complete reaction can be described in the following eqs 1 to 4. The overall photocatalytic CO_2 reduction is a complex and difficult reaction process than the water splitting reaction. In the photocatalytic CO_2 reduction process, the photogenerated holes migrate to the surface and cannot be ignored. At the surface of the Cu/GO photocatalyst, the photogenerated holes may react with adsorbed water to produce oxygen due to the valence band position of the Cu/GO photocatalyst, but this reaction is difficult to analyze quantitatively. We assume that the accumulation of holes on the GO surface may lead to an increase in surface recombination and thus decreasing the product formation after certain period of irradiation time

$$GO + h\nu \rightarrow GO(e^- + h^+) \quad (1)$$

$$H_2O + h^+ \rightarrow 2H^+ + 2e^- + 1/2O_2 \qquad E^0 = -0.82\ V \quad (2)$$

$$CO_2 + 6H^+ + 6e^- \rightarrow CH_3OH + H_2O \qquad E^0 = -0.38\ V \quad (3)$$

$$2CO_2 + 10H^+ + 10e^- \rightarrow CH_3CHO + 3H_2O \qquad E^0 = -0.36\ V \quad (4)$$

Based on the above reactions, a hypothetical mechanism for the CO_2 photoreduction reaction is proposed for Cu-NPs modified GO composite. The work function and conduction band (CB) energy of the Cu/GO hybrids are illustrated in Figure 4. To determine the work function of the Cu/GO

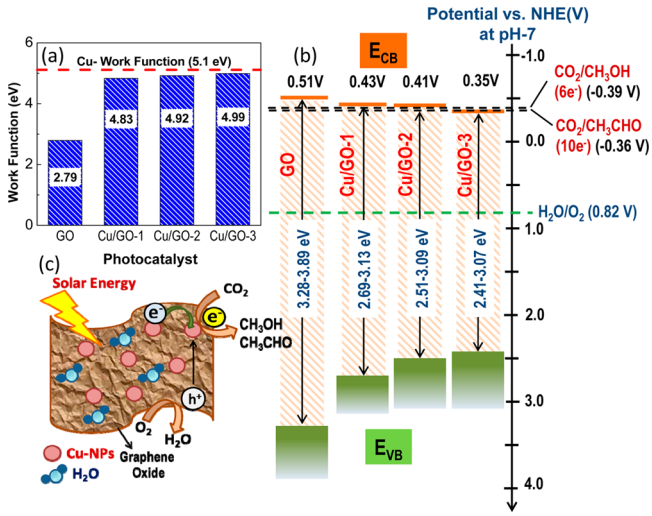

Figure 4. (a) UPS-determined work functions of GO and Cu/GO hybrids and (b) band-edge positions of pristine GO and Cu/GO hybrids in compared with CO_2/CH_3OH and CO_2/CH_3CHO formation potential. (c) Schematic photocatalytic reaction mechanism.

hybrids, UV photoelectron spectroscopy (UPS) measurements were performed, as shown in Supporting Information Figure S7. Interestingly, it can be observed in Figure 4a that with the increasing Cu loading, the work function of Cu/GO hybrid continuously increases. This phenomenon can be attributed to the spontaneous transfer of electrons from GO to Cu-NPs, resulting in shifting of the Fermi level to more negative potential. Because the Fermi level of Cu-NPs is lower than the CB of GO, the photoexcited electrons can easily transfer from the GO CB to the Cu-NPs, whereas photogenerated VB holes remain in GO. It is likely that the accumulated electrons on Cu-NPs participate in CO_2 reduction, whereas holes in GO lead to the oxidation reaction. Therefore, charge separation at the GO-Cu/NPs interface and suppression of carrier recombination can be realized, which leads to an enhanced photocatalytic CO_2 reduction on the GO. The observed maxima in hydrocarbon formation on Cu/GO-2 suggest that the position of its CB is optimum for this catalytic reaction. We, thus, postulate that the presence of Cu nanoparticles in Cu/GO-2 tune the position of the CB to an optimum energy for photocatalytic CO_2 reduction.

Besides the enhancement in photocatalytic activity by Cu/GO hybrids, the variation in the production rate of different

dx.doi.org/10.1021/nl503609v | Nano Lett. 2014, 14, 6097−6103

products as a function of Cu-loading is another interesting issue. In order to explain the observed variation in production rates presented in Figure 3, the position of the conduction band in GO, Cu/GO-1, Cu/GO-2, and Cu/GO-3 were calculated based on the onset potential for reduction reaction for these materials (see Supporting Information Figure S8). In Figure 4b, the positions of the valence band-edge in these samples are plotted as a function of onset potential for reduction reaction. The figure clearly shows the feasibility of the multi electron reduction of CO_2 to methanol and acetaldehyde. In contrast, the position of CB in Cu/GO-3 is slightly lower than the CO_2/CH_3OH reduction potential at around −0.35 V, which leads to the preferential production of acetaldehyde with this reaction. Recently, Kuhl et al.[48] have demonstrated in detail the electroreduction mechanism of CO_2 on Cu surface, resulting in a similar product distribution (C1−C2) as observed in the present study. In addition, besides the role of the conduction band position, photocatalytic methanol reforming can also contribute to reduced methanol production in the presence of excess Cu because methanol has lower splitting energy relative to water.[49] In the present Cu/GO composites, the bulk recombination was reduced by presence of metallic Cu nanoparticles. The acceptance of a charge carrier by a metal nanoparticle, however, is strongly related to the size of the nanoparticles because the interfacial electronic states relative to the position of conduction band are a function of the size of the NPs. At 10 wt % Cu-loading on GO, the conduction band position is tuned at such an energy level that it favors selective reduction of CO_2 to a specific product. The size and density of Cu nanoparticles on graphene oxide basal plane highly influenced the photocatalytic CO_2 reduction efficiency. The smaller copper particle with high surface area offered a shorter charge transfer pathway for quick electron trapping. Additionally, the particular case in Cu/GO-2 with 10 wt % Cu nanoparticles provides a better electronic stability as compared to the other Cu/GOs hybrids. We believe that a strong interaction between copper nanoparticles and the graphene oxide occurs, which may improve the catalytic activity. However, further study is needed to understand the mechanism of the change in productivity at excess Cu content.

In conclusion, a series of Cu-NP modified GO photocatalysts have been successfully synthesized by simple microwave process that demonstrated significant enhancement in the photocatalytic activity toward solar fuel production. The Cu/GO-2 composite containing 10 wt % Cu exhibited the highest solar fuel formation rate of 6.84 μmol g-cat^{-1} h^{-1} for photocatalytic CO_2 reduction under visible light irradiation. The photocatalytic CO_2 reduction rate achieved here is 60 times higher than that obtained by the pristine GO and 240 times higher than that by commercial P-25 under visible light. It is believed that the incorporation of Cu-NPs effectively tune the work function of GO, resulting in improved charge separation and thus enhanced photocatalytic reduction of CO_2. The proposed mechanism and the enhanced photocatalytic efficiency of Cu-NPs modified GO provides an opportunity for future development of solar fuel photocatalyst based on GO.

■ ASSOCIATED CONTENT

Supporting Information

Experimental details and additional figures are provided including EDX analysis, XRD, UV−vis, Raman, high-resolution O 1s XPS spectra, work function calculation by UPS analysis, electrochemical determination of conduction band potential, photocatalytic experimental setup. This material is available free of charge via the Internet at http://pubs.acs.org.

■ AUTHOR INFORMATION

Corresponding Authors

*E-mail: chenkh@pub.iams.sinica.edu.tw.
*E-mail: chenlc@ntu.edu.tw.

Notes

The authors declare no competing financial interest.

■ ACKNOWLEDGMENTS

We thank the Ministry of Science and Technology (MOST), Academia Sinica, National Taiwan University and Ministry of Education (MOE), Taiwan and AOARD of AFOSR for financial support. Technical support from Nano-Core, the Core facilities for nanoscience and nanotechnology at Academia Sinica in Taiwan, is acknowledged.

■ REFERENCES

(1) Abelson, P. H. *Science* **1977**, *197*, 941.
(2) Gray, H. B. *Nat. Chem.* **2009**, *1*, 7.
(3) Centi, G.; Perathoner, S. *ChemSusChem* **2010**, *3*, 195−208.
(4) Inoue, T.; Fujishima, A.; Konishi, S.; Honda, K. *Nature* **1979**, *277*, 637−638.
(5) Cook, R. L.; MacDuff, R. C.; Sammells, A. F. *J. Electrochem. Soc.* **1988**, *135*, 3069−3070.
(6) Pan, P.-W.; Chen, Y.-W. *Catal. Commun.* **2007**, *8*, 1546−1549.
(7) Zhou, Y.; Tian, Z.; Zhao, Z.; Liu, Q.; Kou, J.; Chen, X.; Gao, J.; Yan, S.; Zou, Z. *ACS Appl. Mater. Interface* **2011**, *3*, 3594−3601.
(8) Praus, P.; Kozák, O.; Kočí, K.; Panáček, A.; Dvorský, R. *J. Colloid Interface Sci.* **2011**, *360*, 574−579.
(9) Li, P.; Ouyang, S.; Xi, G.; Kako, T.; Ye, J. *J. Phys. Chem. C* **2012**, *116*, 7621−7628.
(10) Izumi, Y. *Coord. Chem. Rev.* **2013**, *257*, 171−186.
(11) Artero, V.; Fontecave, M. *Chem. Soc. Rev.* **2013**, *42*, 2338−2356.
(12) Kočí, K.; Obalová, L.; Lacný, Z. *Chem. Pap.* **2008**, *62*, 1−9.
(13) Dhakshinamoorthy, A.; Navalon, S.; Corma, A.; Garcia, H. *Energy Environ. Sci.* **2012**, *5*, 9217−9233.
(14) Smestad, G. P.; Steinfeld, A. *Ind. Eng. Chem. Res.* **2012**, *51*, 11828−11840.
(15) Navalón, S.; Dhakshinamoorthy, A.; Álvaro, M.; Garcia, H. *ChemSusChem* **2013**, *6*, 562−577.
(16) Balaraman, E.; Gunanathan, C.; Zhang, J.; Shimon, L. J. W.; Milstein, D. *Nat. Chem.* **2011**, *3*, 609−614.
(17) Huff, C. A.; Sanford, M. S. *J. Am. Chem. Soc.* **2011**, *133*, 18122−18125.
(18) Mitton, S. J.; Turculet, L. *Chem.—Eur. J.* **2012**, *18*, 15258−15262.
(19) Courtemanche, M.-A.; Légaré, M.-A.; Maron, L.; Fontaine, F.-G. *J. Am. Chem. Soc.* **2013**, *135*, 9326−9329.
(20) Gopidas, K. R.; Bohorquez, M.; Kamat, P. V. *J. Phys. Chem.* **1990**, *94*, 6435−6440.
(21) Leng, W. H.; Barnes, P. R. F.; Juozapavicius, M.; O'Regan, B. C.; Durrant, J. R. *J. Phys. Chem. Lett.* **2010**, *1*, 967−972.
(22) Pesci, F. M.; Cowan, A. J.; Alexander, B. D.; Durrant, J. R.; Klug, D. R. *J. Phys. Chem. Lett.* **2011**, *2*, 1900−1903.
(23) Hodak, J. H.; Martini, I.; Hartland, G. V. *J. Phys. Chem. B* **1998**, *102*, 6958−6967.
(24) Kamat, P. V. *J. Phys. Chem. Lett.* **2012**, *3*, 663−672.
(25) Dreyer, D. R.; Park, S.; Bielawski, C. W.; Ruoff, R. S. *Chem. Soc. Rev.* **2010**, *39*, 228−240.
(26) Loh, K. P.; Bao, Q.; Eda, G.; Chhowalla, M. *Nat. Chem.* **2010**, *2*, 1015−1024.
(27) Gómez-Navarro, C.; Weitz, R. T.; Bittner, A. M.; Scolari, M.; Mews, A.; Burghard, M.; Kern, K. *Nano Lett.* **2007**, *7*, 3499−3503.

(28) Mathkar, A.; Tozier, D.; Cox, P.; Ong, P.; Galande, C.; Balakrishnan, K.; Leela Mohana Reddy, A.; Ajayan, P. M. *J. Phys. Chem. Lett.* **2012**, *3*, 986−991.
(29) Krishnamoorthy, K.; Mohan, R.; Kim, S.-J. *Appl. Phys. Lett.* **2011**, *98*, 244101.
(30) Su, C.; Acik, M.; Takai, K.; Lu, J.; Hao, S.-j.; Zheng, Y.; Wu, P.; Bao, Q.; Enoki, T.; Chabal, Y. J.; Ping Loh, K. *Nat. Commun.* **2012**, *3*, 1298.
(31) An, X.; Yu, J. C. *RSC Adv.* **2011**, *1*, 1426−1434.
(32) Xiang, Q.; Yu, J.; Jaroniec, M. *Chem. Soc. Rev.* **2012**, *41*, 782−796.
(33) Li, Q.; Guo, B. D.; Yu, J. G.; Ran, J. R.; Zhang, B. H.; Yan, H. J.; Gong, J. R. *J. Am. Chem. Soc.* **2011**, *133*, 10878−10884.
(34) Yeh, T.-F.; Syu, J.-M.; Cheng, C.; Chang, T.-H.; Teng, H. *Adv. Fun. Mater.* **2010**, *20*, 2255−2262.
(35) Hsu, H.-C.; Shown, I.; Wei, H.-Y.; Chang, Y.-C.; Du, H.-Y.; Lin, Y.-G.; Tseng, C.-A.; Wang, C.-H.; Chen, L.-C.; Lin, Y.-C.; Chen, K.-H. *Nanoscale* **2013**, *5*, 262−268.
(36) Varghese, O. K.; Paulose, M.; LaTempa, T. J.; Grimes, C. A. *Nano Lett.* **2009**, *9*, 731−737.
(37) Tseng, I. H.; Wu, J. C. S. *Catal. Today* **2004**, *97*, 113−119.
(38) Nilius, N.; Wallis, T. M.; Ho, W. *Science* **2002**, *297*, 1853−1856.
(39) Hori, Y.; Murata, A.; Takahashi, R. *J. Chem. Soc., Faraday Trans. 1* **1989**, *85*, 2309−2326.
(40) Hori, Y.; Takahashi, R.; Yoshinami, Y.; Murata, A. *J. Phys. Chem. B* **1997**, *101*, 7075−7081.
(41) Gattrell, M.; Gupta, N.; Co, A. *J. Electroanal. Chem.* **2006**, *594*, 1−19.
(42) Vilar-Vidal, N.; Blanco, M. C.; López-Quintela, M. A.; Rivas, J.; Serra, C. *J. Phys. Chem. C* **2010**, *114*, 15924−15930.
(43) Ghodselahi, T.; Vesaghi, M. A.; Shafiekhani, A. *J. Phys. D: Appl. Phys.* **2009**, *42*, 015308.
(44) Koroteev, V. O.; Bulusheva, L. G.; Asanov, I. P.; Shlyakhova, E. V.; Vyalikh, D. V.; Okotrub, A. V. *J. Phys. Chem. C* **2011**, *115*, 21199−21204.
(45) Rasko, J.; Solymosi, F. *J. Phys. Chem.* **1994**, *98*, 7147−7152.
(46) Conway, B. E.; Jerkiewicz, G. *Electrochim. Acta* **2000**, *45*, 4075−4083.
(47) Shi, C.; Hansen, H. A.; Lausche, A. C.; Norskov, J. K. *Phys. Chem. Chem. Phys.* **2014**, *16*, 4720−4727.
(48) Kuhl, K. P.; Cave, E. R.; Abram, D. N.; Jaramillo, T. F. *Energy Environ. Sci.* **2012**, *5*, 7050−7059.
(49) Choi, H.-J.; Kang, M. *Int. J. Hydrogen Energy* **2007**, *32*, 3841−3848.

dx.doi.org/10.1021/nl503609v | *Nano Lett.* 2014, 14, 6097−6103